Investigations of Strong Hydrogen Bonding in $(ROH)_n\cdots FHF^-$ ($n = 1, 2$ and R = H, CH_3, C_2H_5) Clusters via High-Pressure Mass Spectrometry and Quantum Calculations

Robert J. Nieckarz,[†] Nathan Oldridge,[†] Travis D. Fridgen,[‡] Guanping P. Li,[§] Ian P. Hamilton,[||] and Terry B. McMahon*,[†]

Department of Chemistry, University of Waterloo, Waterloo, Ontario N2L 3G1, Canada, Department of Chemistry, Memorial University of Newfoundland, St. John's, NL A1B 3X9, Canada, SICAS Center, State University of New York Oneonta, Oneonta, New York 13820, USA, and Department of Chemistry, Wilfrid Laurier University, Waterloo, ON N2L 3C5, Canada

Received: August 8, 2008; Revised Manuscript Received: October 30, 2008

An examination of strong hydrogen bonds found in $(ROH)_n\cdots FHF^-$ clusters ($n = 1$ and 2; R = H, CH_3, C_2H_5) is presented. Excellent agreement is observed between thermochemical values obtained from high-pressure mass spectrometric measurements and those predicted from MP2(full)/6-311++G(d,p)//B3LYP/6-311++G(d,p) calculations. Calculated structures are examined, and insight into the geometric nature of the bonding for these systems is obtained. In the case of water binding to FHF^-, it was found that the large entropic advantage of one particular structure, which was not the most enthalpically favored, was significant enough to make it the predominant species within the ion source. In the case of methanol solvation, no evidence of secondary interaction of the methyl group and any other moiety could be found. The structural details revealed from calculations of the ethanol-solvated clusters indicate that secondary interactions between the terminal methyl group and FHF^- have an impact on the length of the FHF and OHF bonds.

Introduction

The extent to which hydrogen bonding plays a fundamental role in chemical and biological systems has warranted investigations into their fundamental nature. One hydrogen-bonded system which has received much attention is that of the hydrogen bihalides, XHY^- (X,Y = F, Cl, Br, or I), whose simplicity allows for (sometimes excruciatingly) in-depth examinations of these prototypical short strong hydrogen bonds (SSHBs). The well-documented thermochemical,[1−10] spectroscopic,[11−20] and geometric[8,10,11,14,17,19] properties of these linear triatomic anions, as well as the acquisition of a fundamental understanding of the factors influencing their bonding, enable the establishment of a basis for the examination of more complex hydrogen bonding systems.

Of the XHY^- species, the bifluoride anion, FHF^-, has the strongest hydrogen bond in the group, and as such, has been extensively examined. The vibrational levels of this anion have been reported by Kawaguchi and Hirota,[11] and its equilibrium F−F bond distance was determined to be 2.278 Å. High-level computational studies have shown FHF^- to be linear with a symmetrically shared proton, giving it $D_{\infty h}$ symmetry. Wenthold and Squires determined the strength of this bond to be 191.6 kJ mol^{-1} via kinetic method measurements of flowing afterglow current image diffraction experiments, which, in terms of strength, places this hydrogen bond in the covalent regime. Despite the attention this simple triatomic anion has received, it is quite surprising to note that investigations of clusters involving this ideal ionic hydrogen bond are limited to a short list of computational studies. Investigations into the stepwise clustering of FHF^- with $(ROH)_n$ ($n = 1,2$ and R = H, C_2H_5) have been performed by Li and Hamilton et al.[21−23] and showed that upon solvation the F−F distance becomes elongated and the proton in FHF^- is no longer symmetrically shared. Moreover, these two characteristics were indicative of a weakening of the FHF hydrogen bond, which, in the case of two water attachments, was by as much as 79.1 kJ mol^{-1}.

A closer look at the changes in hydrogen bond geometric properties seen in the reported structures of Li and Hamilton et al. were consistent with predictions of the traditional model of hydrogen bonding. By consideration of an ionic hydrogen bond to be comprised of a proton-donating AH moiety and a proton accepting B^- moiety, $AH\cdots B^-$, if the acid strength of AH and the basicity of B^- are raised, the hydrogen bond strength and linearity will increase while bond length will decrease. (Note that in this manuscript the term acid strength denotes proton donating ability. This is to be differentiated from the thermochemical definition of acidity, which is the free energy associated with deprotonation of an acid, AH, such that a higher value of acidity denotes a lower acid strength.) For instance, the addition of one water molecule to FHF^- was reported to lengthen the F−F distance by 0.027 Å and cause a slight bending, ∠FHF = 179.2°, at the B3LYP/6-311++G(d,p) level of theory.[23] This lengthening can be attributed to the formation of an $OH\cdots F$ hydrogen bond to FHF^-, causing a weakening of the basicity of the F^- moiety.

Another observation from the calculations of Li and Hamilton et al. was the presence of several isomers (and/or low-lying transition states) of similar binding energy for each cluster examined. Any $FHF^-\cdots(ROH)_n$ clusters that are created under thermodynamic conditions are expected to consist of a distribution of accessible isomers and each isomer's number density will be determined by Boltzmann statistics. In such cases, entropic effects caused from the presence of a mixture of isomers can be expected whose contribution would be dependent on both

* To whom correspondence should be addressed. Phone: (519) 888-4591. Fax: (519) 746-0435. Email: mcmahon@uwaterloo.ca.
[†] University of Waterloo.
[‡] Memorial University of Newfoundland.
[§] State University of New York Oneonta.
[||] Wilfrid Laurier University.

10.1021/jp8071074 CCC: $40.75
Published on Web 01/05/2009

the mole fraction of each isomer, as well as the number of different isomers present. An estimate of the contribution of the entropy of mixing, ΔS°_{mix}, is provided in eq 1

$$\Delta S^\circ_{mix} = -R\sum_{i=1}^{N} x_i \ln(x_i) \quad (1)$$

where N represents the number of different isomers present, x_i represents the mole fraction of each isomer, and R is the ideal gas constant. Such a treatment has recently been applied by Akrour et al. in the investigation of neutral and protonated 2,4-pentanedione, 2,5-hexanedione, and methyl acetoacetate using the kinetic method.[24] To compensate for this effect, an a priori knowledge of all isomers present within the system is required; otherwise, it can generally be noted that any ΔS°_{mix} term would be contained within the observed ΔS°_{rxn}. Since $0 \le x_i \le 1$, ΔS°_{mix} is always ≥ 0, therefore any comparison of a measured ΔS°_{mix} to one calculated for a single isomer would show the measured value to be more positive.

To complement the vast amount of literature available, a high-pressure mass spectrometric (HPMS) study of the stepwise clustering of FHF^- with $(ROH)_n$ solvents has been performed, where $n = 1$, 2 and R = H, CH_3, C_2H_5. Experimental gas-phase thermochemical data pertaining to these systems have been measured and compared to ab initio and density functional theory calculations for various structures of interest. These studies provide further insight into the nature of the SSHB, the importance of which warrants thorough investigation of this hydrogen bond-rich system.

Experimental Methods

All thermodynamic measurements were made using a high-pressure mass spectrometer configured around a VG 8-80 single magnetic sector mass analyzer and a home-built pulsed-ionization high pressure ion source, which has been described in detail elsewhere.[25]

A mixture of 1% NF_3 in CH_4 and varying amounts of the desired protic solvents (solvent partial pressure between 0.01 and 1% of total pressure) was flowed into the ion source at pressures between 6 and 7 torr and temperatures between 40 and 140 °C, depending on the equilibrium reaction being examined. NF_3, CH_4 (99.97% purity), CH_3OH (99.8% purity), and C_2H_5OH were purchased from Ozark-Mahoning, Praxair, Sigma Aldrich, and Commercial Alcohols Inc., respectively, and used as supplied without any further purification, while any H_2O used was purified using a Milli-Q filtration system. Upon bombardment of this reactant gas mixture with a pulsed electron beam of 2 kV, defined by 60-μs long bursts with a period of 60 ms, the desired anionic species were produced within the ion source through the series of ion molecule reactions proposed below, eqs 2−6.

Initial electron bombardment of CH_4 liberates hydrogen atoms and two low-energy secondary electrons, eq 2.[26] These secondary electrons can combine with NF_3 and, through the process of dissociative electron capture, form an abundance of F^-, eq 3,[27] while the hydrogen atoms formed in eq 2 can abstract fluorine from another molecule of NF_3 to form HF,[28] eq 4. The highly exothermic association[1] of F^- and HF leads to the formation of FHF^-, eq 5. Once FHF^- has been formed it is free to undergo a sequential solvation process with ROH, eq 6, where R = H, CH_3, or C_2H_5 and $n = 1$ and 2.

$$CH_4 + e^- \rightarrow CH_3^+ + H^\bullet + 2e^- \quad (2)$$

$$NF_3 + e^- \rightarrow F^- + NF_2^\bullet \quad (3)$$

$$F_2NF + H^\bullet \rightarrow HF + NF_2^\bullet \quad (4)$$

$$F^- + HF \rightarrow FHF^- \quad (5)$$

$$(ROH)_{n-1}\cdot\cdot\cdot FHF^- + ROH(\rightleftharpoons)(ROH)_n\cdot\cdot\cdot FHF^- \quad (6)$$

At the experimental temperatures and pressures used, all newly formed hot ions undergo approximately 10^8 collisions before diffusing out of the ion source and being accelerated onto the detector, thus ensuring that all species had been thermalized to the known temperature of the ion source (estimated using the Langevin equation for collisional rate constants).

A typical $\log_{10}$(intensity)−time profile is depicted in Figure 1 and was collected for the pair of ions involved in eq 6, while the inset shows typical normalized intensity−time profiles. Each plot was the result of an accumulation of ion intensity as a function of time after 2000 successive electron beam pulses. The time required for the ion formation process outlined in eqs 2−6 is reflected in the collected profiles as a 0.5-ms delay between the end of the electron beam pulse ($t = 0$ ms) and the onset of the first observed ion signals. From these intensity-time profiles it can be seen that equilibrium is reached approximately 1.5 ms after the electron beam is turned off, or approximately 1 ms after the ions of interest first appear in the source.

An operational form of the thermodynamic equilibrium constant associated with eq 6 is given below as a function of ion intensity and neutral partial pressures, where $P_0 = 1$ bar, eq 7.

$$K_{eq} = \frac{I_{(ROH)_n\cdots FHF^-}}{I_{(ROH)_{n-1}\cdots FHF^-}\cdot P_{ROH}}\cdot P_0 \quad (7)$$

By taking the ratio of product to reactant ion intensities during the period in which the two ions were in equilibrium (after 1.5 ms) and dividing by the partial pressure of the neutral solvent gas, a measure of the equilibrium constant at a given temperature was obtained. According to eq 8 (the van't Hoff equation), when K_{eq} is measured at various temperatures, information about the change in enthalpy and entropy for a given equilibrium process is obtained. Provided that no significant changes in heat capacity or any major shift in isomeric distribution occurs over a particular temperature range, a plot of $\ln(K_{eq})$ vs T^{-1} can be expected to be linear with enthalpy change found from the slope and entropy change found from the intercept

$$\ln(K_{eq}) = -\frac{\Delta H_{rxn}^\circ}{RT} + \frac{\Delta S_{rxn}^\circ}{R} \quad (8)$$

Six to ten measurements of K_{eq} were obtained at each temperature, and the standard deviation displayed as error bars for each point as shown in the resulting van't Hoff plots. Temperature measurements were performed using a J-type thermocouple with an accuracy of ±1 K. Estimated errors of ± 2.0 kJ mol^{-1}, ±10 J K^{-1} mol^{-1}, and ±4.1 kJ mol^{-1} in ΔH°_{rxn}, ΔS°_{rxn}, and ΔG°_{298}, respectively, are based on the propagation of uncertainties in temperature and pressure measurements for the experiment.

Calculations were performed to complement the HPMS measurements and gain further insight into the energetic and structural properties of the anion−protic solvent clustering process. For each species involved in eq 6, geometry optimizations and frequency calculations were performed using density functional theory (DFT). The hybrid functional B3LYP, of

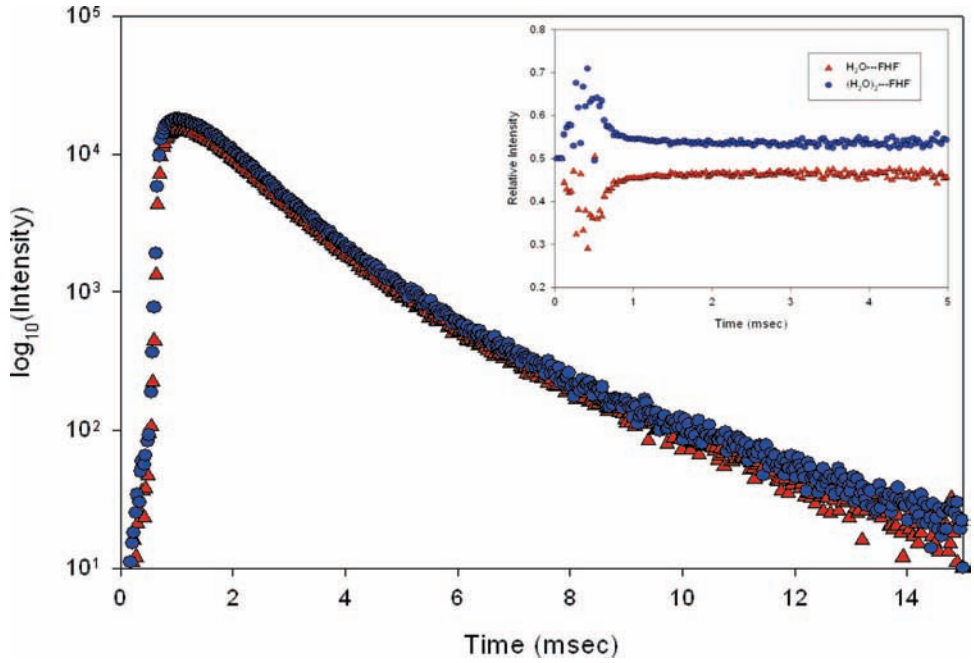

Figure 1. Typical $\log_{10}$(intensity)−time profiles for the ion clusters of FHF^- with one and two water molecules. Inset: Normalized intensity−time profiles.

Becke, Lee, Yang, and Parr, in conjunction with the 6-311++G(d,p) basis set was employed. The electronic energy for each of the previously optimized structures were then computed using fully correlated Møller−Plesset second order perturbation theory (MP2) and the 6-311++G(d,p) basis set. The combination of B3LYP geometry optimizations and fully correlated MP2 calculations results in accurate structural details and electronic energies.[29] All geometry optimization, electronic energy, and statistical thermodynamic calculations were performed using the Gaussian 03 software package[30] with no scaling of frequencies, while all molecular structures were generated using GaussView 3.0.[31]

Values for ΔH°_{rxn} and ΔS°_{rxn} associated with eq 6 were obtained by taking the differences between products and reactants for various calculated properties (supermolecular approach). Standard changes in enthalpy were computed according to eq 9

$$\Delta H^\circ_{rxn} = \Delta E^{elec} + \Delta E^{vib} + \Delta E^{rot} + \Delta E^{trans} + \Delta ZPE + w \quad (9)$$

where ΔE^{elec}, ΔE^{vib}, ΔE^{rot}, and ΔE^{trans} are the differences in electronic, vibrational, rotational, and translational energies between products and reactants, respectively, ΔZPE is the difference in zero point energies, and w is the pressure−volume work done in going from two moles of reactant gas to one mole of product gas. For eq 6, $w = -RT$. Standard entropy changes were computed according to eq 10

$$\Delta S^\circ_{rxn} = \sum_{products} S^\circ_i - \sum_{reactants} S^\circ_j \quad (10)$$

where $\sum_{products} S^\circ_i$ and $\sum_{reactants} S^\circ_j$ represent the sums of translational, electronic, vibrational, and rotational entropies over all product and reactant species, respectively.

Once ΔH°_{rxn} and ΔS°_{rxn} are determined, the change in Gibbs free energy is determined via eq 11,

$$\Delta G^\circ_T = \Delta H^\circ_{rxn} - T\Delta S^\circ_{rxn} \quad (11)$$

In all systems examined, several thermodynamically accessible isomers and rotamers exist on the potential energy surface for each cluster. Only the thermochemical properties of those structures found to be of importance (i.e., enthalpically, entropically, or ergonically favorable species) are reported below.

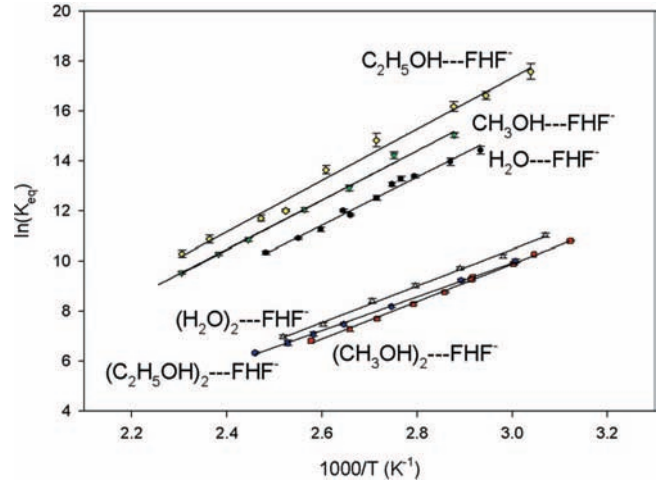

Figure 2. van't Hoff plots for the sequential clustering of one and two water, methanol, and ethanol molecules to FHF^-.

Results and Discussion

3.1. $(H_2O)_{n-1}\cdots FHF^- + H_2O \rightleftharpoons (H_2O)_n\cdots FHF^-$. The van't Hoff plots obtained for the stepwise clustering of one and two water molecules to FHF^- are shown in Figure 2, and associated thermochemical properties, both measured and calculated, are reported in Table 1. ΔH°_{rxn} and ΔS°_{rxn} for the addition of the first water molecule to FHF^- were determined to be -78.6 ± 2.0 kJ mol^{-1} and -107.9 ± 10.0 J K^{-1} mol^{-1}, respectively, via HPMS, while calculations determine ΔH°_{rxn} to be -68.7 kJ mol^{-1} and ΔS°_{rxn} to be -86.6 J K^{-1} mol^{-1}. By use of both the HPMS data and calculated values, changes in Gibbs free energies at 298 K were determined (via eq 11) to be -46.4 ± 4.1 kJ mol^{-1} and -42.8 kJ mol^{-1}, respectively. Good agreement exists between theory and experiment for the thermochemical data obtained. The reported ΔH°_{rxn} values

TABLE 1: Measured (HPMS) and Calculated [MP2(full)/6-311++G(d,p)//B3LYP/6-311++G(d,p)] Thermochemical Properties for Examined Clustering Processes

reaction	ΔH°_{rxn} (kJ mol^{-1})	ΔS°_{rxn} (J K^{-1} mol^{-1})	ΔG°_{298} [†] (kJ mol^{-1})	structure
$FHF^- + (H_2O) \rightleftharpoons (H_2O)FHF^-$	-78.6 ± 2.0	-107.9 ± 10.0	-46.4 ± 4.1	HPMS
	-68.7	-86.6	-42.8	3I
$(H_2O)FHF^- + H_2O$ ($\rightleftharpoons$) $(H_2O)_2FHF^-$	-60.7 ± 2.0	-95.0 ± 10.0	-32.4 ± 4.1	HPMS
	-58.9	-96.2	-30.2	3III
	-59.9	-142.2	-17.5	3II
$FHF^- + CH_3OH \rightleftharpoons (CH_3OH)FHF^-$	-81.3 ± 2.0	-108.1 ± 10.0	-49.1 ± 4.1	HPMS
	-73.2	-84.5	-48.0	4I
$(CH_3OH)FHF^- + CH_3OH$ ($\rightleftharpoons$) $(CH_3OH)_2FHF^-$	-64.0 ± 2.0	-104.9 ± 10.0	-32.7 ± 4.1	HPMS
	-61.2	-106.3	-29.6	4II
	-56.6	-97.2	-27.6	4III
$FHF^- + C_2H_5OH \rightleftharpoons (C_2H_5OH)FHF^-$	-86.4 ± 2.0	-111.1 ± 10.0	-53.3 ± 4.1	HPMS
	-76.4	-92.1	-48.9	5II
	-77.6	-101.4	-47.4	5I
$(C_2H_5OH)FHF^- + C_2H_5OH$ ($\rightleftharpoons$) $(C_2H_2OH)_2FHF^-$	-56.5 ± 2.0	-86.8 ± 10.0	-30.6 ± 4.1	HPMS
	-62.6	-111.3	-29.4	5III
	-60.5	-129.5	-21.9	5IV

[†] $\Delta G_T = \Delta H^\circ_{rxn} - T\Delta S^\circ_{rxn}$.

TABLE 2: Summary of Important Geometric Properties of FHF^- and Several Solvated FHF^- Clusters

structure (figure)	F−F (Å)	H−F (Å)	∠FHF (deg)	F−O (Å)	F−H (Å)	∠FHO (deg)	source
FHF^-	2.278						[a]
	2.294	1.147	180.0				[b]
$H_2O\cdots FHF^-$ (3I)	2.321	1.274	179.21	2.605	1.611	172.18	[c]
	2.321	1.274	179.2	2.605	1.611	172.2	[b]
$(H_2O)_2\cdots FHF^-$ (3II)	2.301	1.231	175.78	2.846, 2.589	1.894, 1.596	164. 73, 171.48	[c]
	2.301	1.226	177	2.824, 2.579	1.868, 1.579	166, 176	[b]
$(H_2O)_2\cdots FHF^-$ (3III)	2.353	1.339	180.00	2.656	1.677	169.15	[c]
$CH_3OH\cdots FHF^-$ (4I)	2.330	1.293	179.65	2.570	1.573	173.54	[c]
$(CH_3OH)_2\cdots FHF^-$ (4II)	2.368	1.364	180.00	2.633	1.651	171.62	[c]
$(CH_3OH)_2\cdots FHF^-$ (4III)	2.283	1.142[e]	179.73	2.647[e]	1.666[e]	173.09[e]	[c]
$C_2H_5OH\cdots FHF^-$ (5I)	2.322	1.278	178.42	2.587	1.593	172.86	[c]
	2.305	1.268		2.345	1.542	173.6	[d]
$C_2H_5OH\cdots FHF^-$ (5II)	2.332	1.299	179.36	2.575	1.584	170.44	[c]
$(C_2H_5OH)_2\cdots FHF^-$ (5III)	2.370	1.367	180.00	2.642	1.661	170.90	[c]
$(C_2H_5OH)_2\cdots FHF^-$ (5IV)	2.281	1.140	180.00	2.673	1.693[e]	172.23[e]	[c]

[a] Reference 11. [b] Reference 23. [c] MP2(full)/6-311++G(d,p)//B3LYP/6-311++G(d,p) [d] Reference 21. [e] Average value.

determined in this study are consistent with the binding energy of 62.3 kJ mol^{-1} reported by Li et al.[23] with any discrepancy between values being explained by differences in calculation methods employed.

The optimized geometry and related structural properties for the most favorable species of $H_2O\cdots FHF^-$ are shown as structure 3I and are consistent with the structure reported by Li et al.[23] Pertinent bond lengths and angles associated with the various calculated monosolvated structures, among others, are reported in Table 2. While the total F−F bond distance of 2.321 Å remains relatively unchanged compared to the unclustered anion (F−F bond distance is 2.278 Å[11] in FHF^-), the addition of H_2O to FHF^- causes the proton in FHF^- to shift to a final position 1.274 Å away from the site of solvent molecule attachment and causes a change in the FHF bond angle to 179.2°, ($\angle FHF = 180.0°$ in FHF^-). The newly formed OHF bond between water and FHF^- possesses a bond angle of 172.2° and a total O−F bond distance of 2.605 Å. Upon close inspection, these geometric details provide information regarding the relative strengths of these hydrogen bonds and are rationalized when simple acidity and basicity arguments are considered.

If FHF^- is envisioned to be constructed of a proton-accepting F^- and a proton-donating HF group, the strongest, shortest, and most linear hydrogen bond will be formed when the gas-phase basicity of F^- and gas-phase acidity of HF are strongest. Unsolvated FHF^- has been shown to be perfectly symmetric, and because of the indistinguishability of the fluorines, it is not possible to immediately assign the title of proton-accepting or proton-donating to either moiety in FHF^-. However, upon addition of the first solvent molecule (in this case water) the two fluorines in FHF^- become distinguishable. The fluorine involved in the newly formed OHF hydrogen bond can be identified as the proton-accepting site in FHF^-, since this new bond will attract electron density toward the site of attachment on FHF^-, giving it properties more similar to F^- than HF. The formation of the OHF hydrogen bond weakens the basicity of the F^- moiety, causing the observed lengthening of the F−F distance when unclustered FHF^- is compared to structure 3I. Should the basicity of this proton-accepting fluorine weaken even further, a further increase in the FHF bond length would be observed. This is exactly what is observed upon the addition of a second water molecule, as discussed below. Since the gas phase acidity of HF ($\Delta_{acid}G^\circ = 1529.3$ kJ mol^{-1})[32] is stronger than that of water ($\Delta_{acid}G^\circ = 1605.4$ kJ mol^{-1}),[33] the FHF hydrogen bond is expected to be stronger than the OHF hydrogen bond. This is supported by the fact that the total O−F distance observed in 3I is larger than the F−F distance, and the OHF bond angle of 172.18° is less linear than the FHF bond angle of 179.21°.

For the addition of a second water molecule onto monosolvated FHF^-, ΔH°_{rxn} and ΔS°_{rxn} were measured to be -60.7 ± 2.0 kJ mol^{-1} and -95.0 ± 10.0 J K^{-1} mol^{-1}, respectively, and

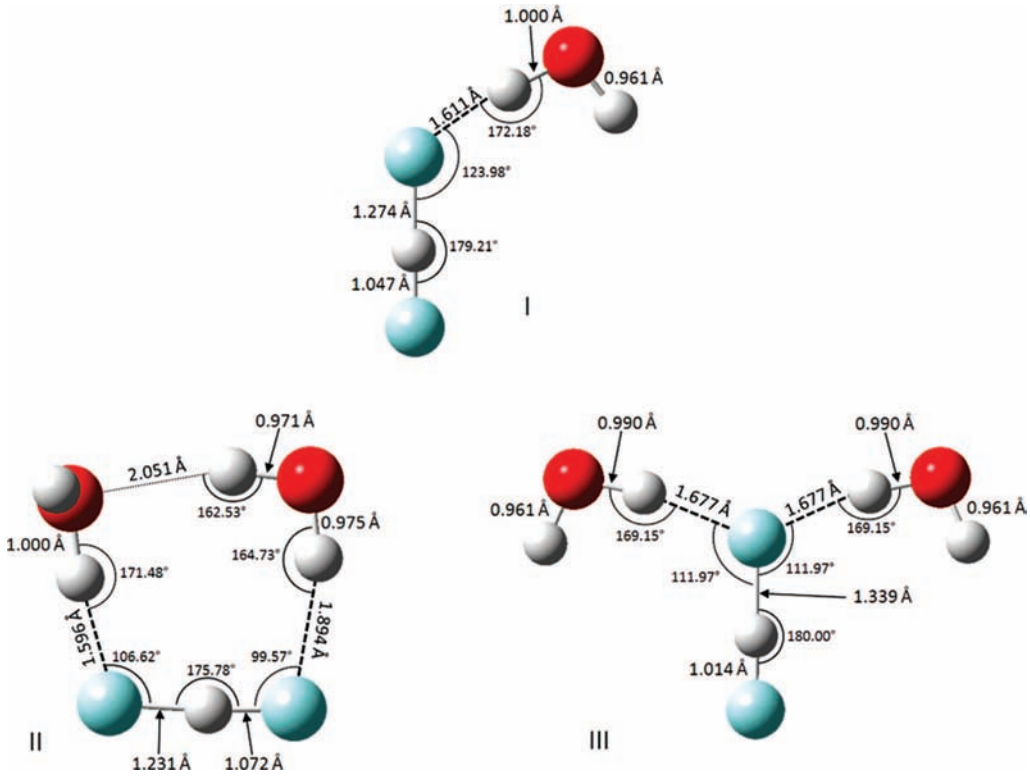

Figure 3. Structures and geometric properties of $FHF^- \cdots (H_2O)_n$ clusters, $n = 1$ and 2.

ΔG°_{298} was determined to be -32.4 ± 4.1 kJ mol^{-1}. These values are as expected, noting the decrease in both exothermicity and exergonicity for the addition of the subsequent water molecule.

From a computational standpoint, several isomers of doubly solvated FHF^-, each possessing similar enthalpies of formation, can be obtained. This has been demonstrated by Li et al. in their presentation of three such structures.[22] Structure 3II reports the most enthalpically favorable structure for the dihydrated FHF^- cluster and is consistent with the most energetically stable structure reported by Li et al., while 3III reports a slightly less enthalpically favorable isomer of this cluster. Rotamers of these two structures can be obtained via rotations of any combination of water molecules about the axis defined by the H−F bond between H_2O and FHF^-. A detailed discussion of such isomers will not be given here, as some of their energetic properties have been investigated previously[22] and were determined to be very similar (within 0.5 kJ mol^{-1}) to the most stable rotamers reported in Figure 3. When left unaccounted for, the presence of these rotamers leads to an increase in the measured value of ΔS°_{rxn}, as discussed in section 2. This is demonstrated upon comparison of entropy changes reported in Table 1 for the addition of the first and second water molecules, noting the higher value of ΔS°_{rxn} for the more isomerically rich dihydrated cluster. Measured and calculated thermodynamic properties for the formation of important clusters of dihydrated FHF^- are compared in Table 1. It is interesting to note that, when entropic and enthalpic arguments are considered and ΔG°_{298} values are compared, structure 3III clearly emerges as the most thermodynamically favorable isomer. A comparison of the calculated thermodynamic properties of 3III to the measured thermochemical fingerprint obtained from HPMS further exemplifies this point. Such a comparison provides evidence that the thermodynamically favored isomer is the predominant one found within the high pressure ion source and that the second water molecule will exhibit a tendency to attach to the monosolvated FHF^- in the manner shown in 3III. The excellent linearity of the associated van't Hoff plot (Figure 2) only provides further support of this fact, demonstrating the ability of high pressure mass spectrometry to distinguish between isomers, based on their thermochemical properties.

A detailed examination of the geometry of structure 3III provides more insight into the effect of solvation on FHF^-. Observations made of the geometric changes of the monohydrated cluster become even more evident in the case of the dihydrated anion. As seen in 3III, the proton in FHF^- shifts to a final position 1.339 Å away from the point of solvation, 0.065 Å further than for the singly solvated case, making the total F−F distance 2.353 Å. Again this is expected since the basicity of the F^- moiety is weakened even further than in the monohydrated case, and thus a weaker FHF bond is observed. It is interesting to note that attachment of a second solvent molecule to the unclustered end of monosolvated FHF^-, as in the case of the ergonically less favorable 3II, the acid strength of the proton donating fluorine in FHF^- increases and when compared to the monohydrated case, a strengthening of the FHF bond, indicated by a shorter F−F distance of 2.301 Å, is observed. In structure 3III both OHF bond angles are found to be 169.1° and the total O−F distances are 2.656 Å, indicating a weaker interaction than observed in the $n = 1$ cluster. An interesting result of the addition of a second solvent molecule was the restoration of symmetry to FHF^-, indicated by the return of the FHF bond angle to 180° (as is the case found for unclustered FHF^-). This is in contrast to the nonlinear FHF bonds of structures 3I and 3II, for which the bond angles are 179.2° and 175.78°, respectively.

3.2. $(CH_3OH)_{n-1} \cdots FHF^- + CH_3OH \rightleftharpoons (CH_3OH)_n \cdots FHF^-$. The van't Hoff plots for the $n = 1$ and 2 cases of methanol clustering onto FHF^- are shown in Figure 2. From these plots, ΔH°_{rxn} for the first and second addition of methanol were measured to be -81.3 ± 2.0 kJ mol^{-1} and -64.0 ± 2.0 kJ mol^{-1}, while ΔS°_{rxn} for these reactions were determined to be -108.1 ± 10.0 J K^{-1} mol^{-1} and -104.9 ± 10.0 J K^{-1} mol^{-1},

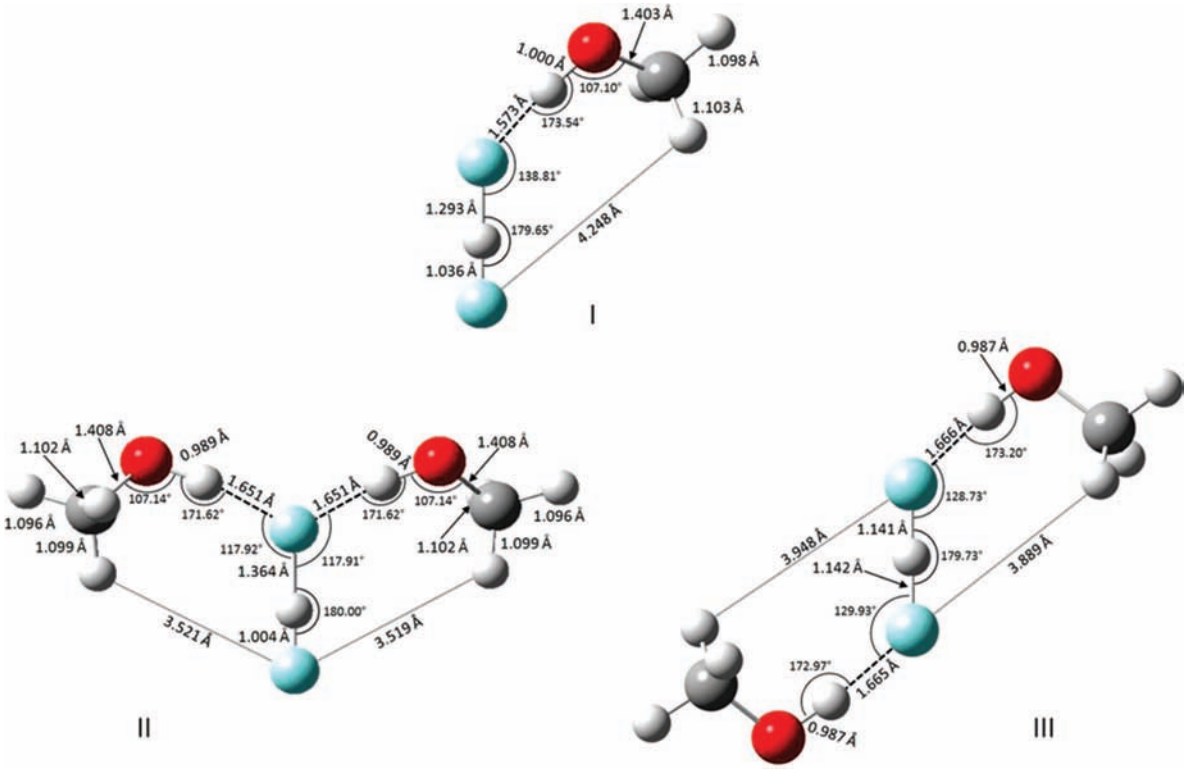

Figure 4. Structures and geometric properties of $FHF^-\cdots(CH_3OH)_n$ clusters, $n = 1$ and 2.

respectively. Equation 11 was employed to determine ΔG°_{298} to be -49.1 ± 4.1 kJ mol^{-1} and -32.7 ± 4.1 kJ mol^{-1}. Calculations performed on this system determined ΔH°_{rxn}, ΔS°_{rxn}, and ΔG°_{298} for the monosolvated case to be -73.2 kJ mol^{-1}, -84.5 J K^{-1} mol^{-1}, and -48.0 kJ mol^{-1}. These values can be found in Table 1, noting a similar level of agreement between measurements and calculations as that observed in the water clusters. In the case of the disolvated cluster, ΔH°_{rxn}, ΔS°_{rxn}, and ΔG°_{298} were determined to be -61.2 kJ mol^{-1}, -106.3 J K^{-1} mol^{-1}, and -29.6 kJ mol^{-1} and are in good agreement with experimental values. This increase in agreement between experimental and calculated data over the monosolvated case is, again, similar to that observed in the water clusters.

Reported in Figure 4 are the lowest energy (and thermodynamically favored) structures calculated for methanol solvated FHF^- clusters. Many of the observations made on these clusters are analogous to those made for the water clusters reported in Figure 3. Rotamers of 4II can be obtained which possess an energy within 1 kJ mol^{-1} of the reported lowest energy structures and can be envisioned as rotations of the methanol about the HF axis of the various OHF hydrogen bonds. Other isomers of the disolvated cluster have been investigated, where attachment of the second methanol takes place on the opposite end of the FHF^-, as seen in structure 4III. A comparison of the calculated thermochemical properties for structures 4II and 4III is given in Table 1. According to calculations, 4III is 4.6 kJ mol^{-1} less enthalpically favorable and 2.0 kJ mol^{-1} less ergonically favorable than structure 4II. This small difference leads to the prediction that both of these isomers, as well as any others of comparable energetics, will contribute significantly to the overall thermochemistry observed within the ion source.

Pertinent bond lengths and angles for structures 4I−III are tabulated in Table 2. The relationship between bond length and bond strength is demonstrated in both 4I and 4II, as the proton in FHF^- is observed to shift to a final position 1.293 and 1.364 Å away from the site of solvation. Total F−F bond distances for the mono- and disolvated clusters are calculated to be 2.330 and 2.368 Å, respectively. The FHF bond angle goes through an evolution similar to that observed for the water clusters. Specifically, addition of the first solvent molecule causes the once linear FHF^- to bend slightly to 179.65°, while addition of the second restores the angle to 180.00. The newly formed OHF hydrogen bond of the monosolvated cluster is characterized by an H−F distance of 1.573 Å, a total O−F distance of 2.570 Å, and ∠OHF = 173.54°. According to calculation, the addition of a second methanol, as shown in structure 4II alters the geometry of the first OHF bond, resulting in two identical OHF bonds with an H−F distance of 1.651 Å, a total O−F distance of 2.633 Å, and ∠OHF = 171.62°. In contrast to structures 3I, 3II, 3III, 4I, and 4II, the observed F−F bond distance found in 4III (2.283 Å) is only 0.005 Å longer than the F−F distance in unsolvated FHF^-.

3.3. $(C_2H_5OH)_{n-1}\cdots FHF^- + C_2H_5OH \rightleftharpoons (C_2H_5OH)_n\cdots FHF^-$. The van't Hoff plots for the clustering of one and two ethanol molecules to FHF^- are shown in Figure 2, with measured and calculated values for the associated processes reported in Table 1. HPMS determined values of ΔH°_{rxn} and ΔS°_{rxn} for the addition of the first ethanol molecule to FHF^- are -86.4 ± 2.0 kJ mol^{-1} and -111.1 ± 10.0 J K^{-1} mol^{-1}, respectively, while calculations determine ΔH°_{rxn} to be -76.4 kJ mol^{-1} and ΔS°_{rxn} to be -92.1 J K^{-1} mol^{-1}. Again, eq 11 was employed and ΔG°_{298} values from HPMS and calculation were determined to be -53.3 ± 4.1 kJ mol^{-1} and -48.9 kJ mol^{-1}, respectively. For the addition of the second molecule of ethanol, HPMS experiments determined ΔH°_{rxn} and ΔS°_{rxn} to be -56.5 ± 2.0 kJ mol^{-1} and -86.8 ± 10.0 J K^{-1} mol^{-1}, respectively, while calculations determined them to be -62.6 kJ mol^{-1} and -111.3 J K^{-1} mol^{-1}. ΔG°_{298} values obtained from HPMS and calculations were found to be -30.6 ± 4.1 kJ mol^{-1} and -29.4 kJ mol^{-1}, respectively. The level of agreement between theory and experiment was found to be of the same high degree of accuracy as noted in the cases of water and methanol.

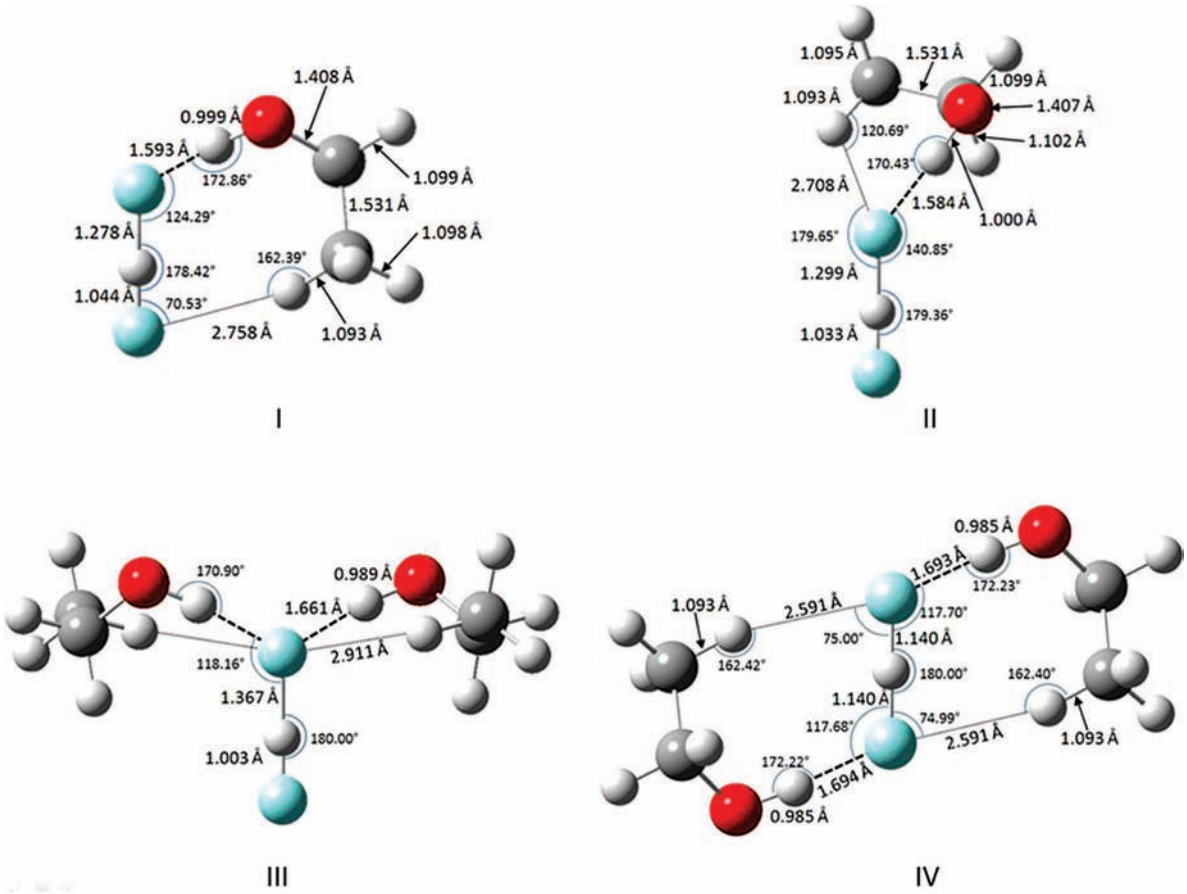

Figure 5. Structures and geometric properties of $FHF^- \cdots (C_2H_5OH)_n$ clusters, $n = 1$ and 2.

As in the cases of water and methanol solvation, many thermodynamically accessible isomers exist for the cluster ions involved in the solvation of FHF^- with C_2H_5OH. Two such isomers have been previously discussed in detail by Hamilton et al.,[21] while structure 5I shows the most enthalpically favorable structure found. The lowest energy structure for the cluster of one ethanol and FHF^- reported by Hamilton at the MP2 level of theory was consistent with the enthalpically favorable structure found in this study at the B3LYP level of theory. A direct comparison between 5I and the structure reported by Hamilton shows all covalent bond lengths to agree to within 0.01 Å, while the noncovalent OHF and CHF interactions to differ by 0.051 and 0.308 Å, respectively. A third, previously unreported isomer, 5II, is also reported and was found to be the most ergonically favorable structure of $C_2H_5OH \cdots FHF^-$. While structure 5II is slightly less enthalpically favorable, an increase in the entropic favorability gives this ion a small ergonic advantage of 1.5 kJ mol^{-1} over 5I. The thermochemical details of 5I and 5II are reported in Table 1. This difference is, however, small and thus a statistical distribution of these two isomers, as well all other accessible isomers, are expected to be found within the high-pressure ion source. Evidence of this can be seen in Table 1 as the measured value of ΔS°_{rxn} is observed to be more positive than the calculated value by nearly 20 J K^{-1} mol^{-1}, as predicted by eq 1.

Inspection of the geometries of these clusters (Table 2) continues to demonstrate the effects of solvation on the strong FHF hydrogen bond. Structure **5I** reveals a smaller proton shift in FHF^-, compared to the methanol solvated counterpart, with the proton sitting a final distance of 1.278 Å away from the fluorine involved in the new OHF bond and $\angle FHF = 178.42°$. This decrease in proton shift from the center can be rationalized by the presence of an additional CHF hydrogen bond between the solvent molecule and FHF^-, taking place on the fluorine not involved with the strong OHF bond. As stated before, if FHF^- is envisioned to be comprised of an HF proton-donating group and an F^- proton-accepting group, this second interaction acts to increase the acid strength of the HF donating group, resulting in a stronger FHF hydrogen bond than that found in the methanol solvated case. Inspection of 5II demonstrates the effect of forming the second interaction to the F^- proton-accepting group. This causes the basicity of this moiety to weaken, and hence, a longer HF distance of 1.299 Å is observed. It is interesting to see that the FHF bond in 5II ($\angle FHF = 179.36°$) retains more of its linearity than does 5I upon solvation. The OHF bonds of both 5I and 5II can be characterized as having O−F distances of 2.587 and 2.575 Å, respectively, H−F distances of 1.593 and 1.584 and a bond angles of 172.86 and 170.43°.

The addition of a second molecule of ethanol to monosolvated FHF^- can be envisioned to take place in two main ways: (1) through the formation of a second strong OHF hydrogen bond to the same fluorine as the first strong OHF bond or (2) through the formation of the second strong OHF bond at the opposite fluorine in FHF compared to the site of attachment of the first ethanol. Structures 5III and 5IV depict the two lowest energy isomers of the aforementioned types for FHF^- disolvated with ethanol, and associated thermochemical data are found in Table 1. Many rotamers of both 5III and 5IV exist, but they will not be discussed here. The observation of an even larger discrepancy between measured and calculated values of ΔS°_{rxn}, reported in Table 1, indicates the presence of an even larger number of isomers within the ion source compared to the disolvated water or methanol clusters. As in the cases of two water and methanol

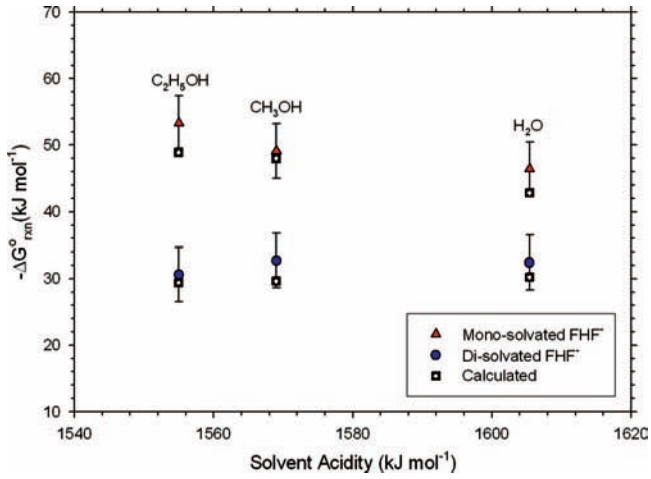

Figure 6. Measured and calculated ergonicity of stepwise formation reactions for $(ROH)_n\cdots FHF^-$ as a function of the gas phase acidity of ROH (n = 1 and 2; R = H, CH_3, C_2H_5). Gas-phase acidities for H_2O, CH_3OH, and C_2H_5OH were obtained in previous works.[33,34]

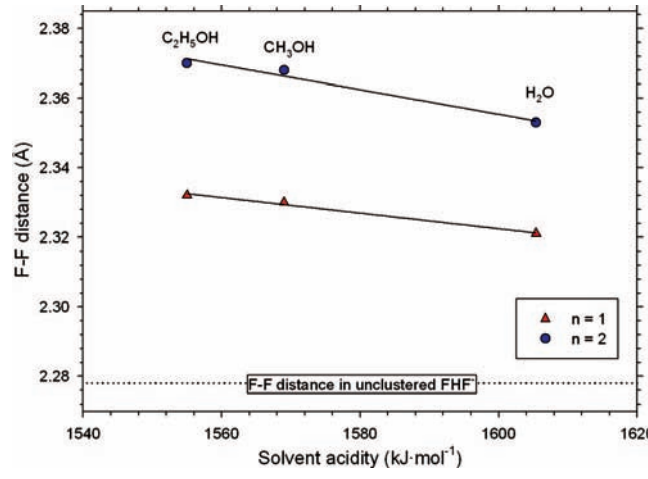

Figure 7. Calculated F−F bond distances in $(ROH)_n\cdots FHF^-$ clusters (n = 1 and 2; R = H, CH_3, C_2H_5) plotted against the gas phase acidity of ROH. Note, only F−F distances for the most ergonically favorable species are plotted. Gas-phase acidities for H_2O, CH_3OH, and C_2H_5OH were obtained in previous works.[33,34]

molecules onto FHF^-, the site of attachment of a second ethanol is most ergonically favorable on the same fluorine possessing the first strong OHF bond, in this case by 7.5 kJ mol^{-1}.

Examination of 5III once again shows the difluorinated proton shift away from the site of solvation to a final equilibrium distance of 1.367 Å. The calculated FHF bond angle of 180.00° and symmetric placement of the two solvent molecules for this ergonically favorable structure give rise to the familiar C_2 point group arrangement that was observed in the disolvated water and methanol systems. Both OHF bonds were determined to have the proton resting at an equilibrium distance of 1.661 Å away from the fluorine with ∠OHF = 170.90°. Structure 5IV, while 7.5 kJ mol^{-1} less favorable ergonically and not considered to be a major constituent within the high pressure ion source, possesses some interesting properties that are worth mentioning. The effect of the highly symmetric double solvation on the FHF bond can be seen in both its linearity and its bond length. The total F−F distance, 2.280 Å, in this isomer is again found to be quite short, 0.002 Å greater than that in bare FHF^- and 0.004 Å shorter than 4III.

3.4. Summary of Thermochemical and Geometric Trends. To better demonstrate the relationship between hydrogen bond strength and the acidity and basicity of all bonding groups involved, several comparative graphs are presented. Figure 6 is a plot of ΔG°_{298} for the addition of a solvent molecule (i.e., the formation of an OHF hydrogen bond) as a function of the gas-phase acidity of the solvent molecule. Both experimentally determined and calculated values for the stepwise solvation of FHF^- with water, methanol, and ethanol are shown, demonstrating the excellent agreement between theory and experiment.

When considering the monosolvation of FHF^-, an expected increase in the hydrogen bond strength is observed as the acid strength of the solvent molecule increases. It can also be noted that this initial solvation of FHF^- weakens the basicity of the proton-accepting fluorine, resulting in all subsequent hydrogen bonds formed (the disolvated cases) to that fluorine being less exergonic.

When considering the disolvated clusters, it is interesting to note that an increase in the experimentally determined exergonicity is observed from water to methanol, while a decrease in exergonicity is observed when the acid strength is further increased to the case of ethanol. This break in the direct relationship between bond strength and solvent acid strength is a manifestation of secondary interactions between the terminal methyl group of ethanol and the fluorine of FHF^-. The presence of this secondary interaction in the monosolvated cluster weakens the basicity of the proton accepting fluorine, demonstrating that even though the acid strength of the solvent molecule may increase; the overall strength of a second OHF hydrogen bond may be lower than expected.

Figure 7 is a plot of the total F−F bond distance in FHF^- as a function of the gas phase acidity of the solvent molecule. Compared to unclustered FHF^-, an increase in F−F bond length is observed upon monosolvation. In both the mono- and disolvated systems, a linear increase in the F−F distance as a function of the acid strength of the solvent exists and can be rationalized as follows. Since the basicity of the fluorine decreases as a result of the newly formed OHF hydrogen bond, a lengthening of all other bonds with which it is involved (the strong hydrogen bond in FHF^-) is expected. Likewise, as acid strength of the solvent increases, the F−F bond distance continues to increase. If a second hydrogen bond is formed to the fluorine (moving vertically within Figure 7, from the monosolvated case to the disolvated case), a further weakening in fluorine basicity occurs, and hence, a large increase in the F−F bond distance is observed. As acid strength of the solvent in the disolvated system increases, so will the F−F distance.

The F−O bond distance found in the most ergonically favored species is plotted against the gas phase acidity of the solvent in Figure 8. As the acid strength of the solvent increases, a stronger hydrogen bond (shorter F−O distance) is expected since the proton donating ability of the hydroxyl will increase. In both the mono- and disolvated cases, this shortening of the F−O distance can be observed when water clusters are compared to those of methanol, however a slight lengthening of the F−O distance is observed when methanol is compared to ethanol. To discern the trends observed here, the effect of secondary interactions must once again be considered. Upon inspection of the equilibrium structure of the ethanol clusters, it can be seen that a secondary interaction between the terminal methyl of ethanol and the same fluorine involved in the strong OHF hydrogen bond exists. This secondary interaction, also responsible for raising the exergonicity of the n = 2 cluster of ethanol onto FHF^- (Figure 7), decreases the basicity of the fluorine and hence results in a slightly longer than expected F−O distance.

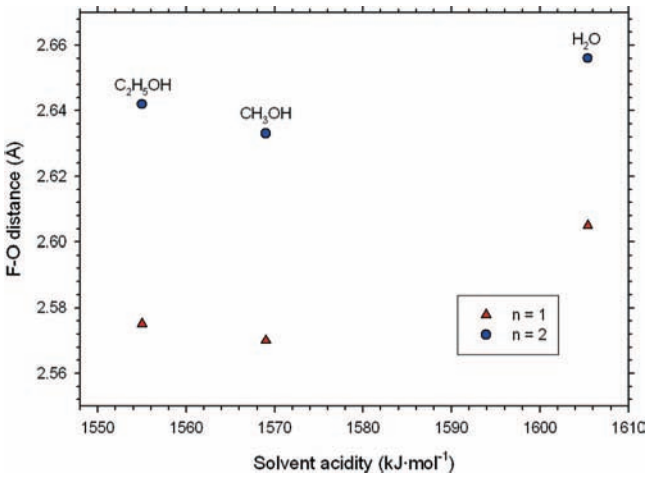

Figure 8. Calculated F−O bond distances in $(ROH)_n\cdots FHF^-$ clusters ($n = 1$ and 2; R = H, CH_3, C_2H_5) plotted against the gas-phase acidity of ROH. Note, only F−O distances for the most ergonically favorable species are plotted. In the case of the doubly solvated clusters, the C_2 symmetry of these clusters reduces the discussion of two separate OHF hydrogen bonds to that of one identical pair (via an 180° rotation) of OHF bonds. Gas-phase acidities for H_2O, CH_3OH, and C_2H_5OH were obtained in previous works.[33,34]

Conclusions

An examination of the strong and very strong hydrogen bonds found in $(ROH)_n\cdots FHF^-$ clusters ($n = 1$ and 2; R = H, CH_3, C_2H_5) has been presented. Very good agreement has been observed between thermochemical values obtained from HPMS measurements and those predicted from MP2(full)/6-311++G(d,p)// B3LYP/6-311++G(d,p) calculations, with all calculated values of the ergonicity falling within the experimental error of ± 4.1 kJ mol^{-1}. Calculated structures were then examined and insight into the geometric bonding nature of these systems was obtained. In the case of water binding to FHF^-, it was found that the large entropic advantage of structure 3III over 3II was significant enough as to make 3III the predominant species found within the ion source. In the case of methanol solvation, no evidence of secondary interaction of the methyl group with any other moiety could be found. The structural details revealed from the ethanol-solvated clusters indicate that if secondary interactions between the terminal methyl group and FHF^- are present, then the consequences of such interactions can be seen in both the strength and the length of the FHF and OHF bonds.

Acknowledgment. The financial support of the Natural Sciences and Engineering Research Council of Canada in the form of Discovery Grants to T.D.F., I.P.H., and T.B.M. and an Undergraduate Student Research Assistantship to N.O. is gratefully acknowledged as is the scholarship support to R.N. by the Ontario Graduate Scholarship fund. The assistance of Melisa Clements in some of the early experiments is also recognized.

Supporting Information Available: Complete citation for ref 30. This information is available free of charge via the Internet at http://pubs.acs.org.

References and Notes

(1) Wenthold, P. G.; Squires, R. R. *J. Phys. Chem.* **1995**, *99*, 2002–2005.
(2) Larson, J. W.; McMahon, T. B. *J. Am. Chem. Soc.* **1983**, *105*, 2944–2950.
(3) Yamdagni, R.; Kebarle, P. *J. Am. Chem. Soc.* **1971**, *93*, 7139–7143.
(4) Rappe, A. K.; Bernstein, E. R. *J. Phys. Chem. A* **2000**, *104*, 6117–6128.
(5) Chojnacki, H. *J. Mol. Struct.* **1997**, *404*, 83–85.
(6) Platts, J. A.; Laidig, K. E. *J. Phys. Chem.* **1996**, *100*, 13455–13461.
(7) Davidson, E. R. *Int. J. Quantum Chem.* **2004**, *98*, 317–324.
(8) Larson, J. W.; McMahon, T. B. *Inorg. Chem.* **1984**, *23*, 2029–2033.
(9) Yamdagni, R.; Kebarle, P. *Can. J. Chem.* **1974**, *52*, 2449–2453.
(10) Rauk, A.; Armstrong, D. A. *Int. J. Quantum Chem.* **2003**, *95*, 683–696.
(11) Kawaguchi, K.; Hirota, E. *J. Chem. Phys.* **1987**, *87*, 6838–6841.
(12) Fridgen, T. D.; Zhang, X. K.; Parnis, J. M.; March, R. E. *J. Phys. Chem. A* **2000**, *104*, 3487.
(13) Rasanen, M.; Seetula, J.; Kunttu, H. *J. Chem. Phys.* **1993**, *98*, 3914.
(14) Frisch, M. J.; Del Bene, J. E.; Binkley, J. S.; Schaefer, H. F., III *J. Chem. Phys.* **1986**, *84*, 2279–2289.
(15) Pivonka, N. L.; Kaposta, C.; Brummer, M.; von Helden, G.; Meijer, G.; Woste, L.; Neumark, D. M.; Asmis, K. R. *J. Chem. Phys.* **2003**, *118*, 5275–5278.
(16) Pivonka, N. L.; Kaposta, C.; von Helden, G.; Meijer, G.; Woste, L.; Neumark, D. M.; Asmis, K. R. *J. Chem. Phys.* **2002**, *117*, 6493–6499.
(17) Elghobashi, N.; Gonzalez, L. *J. Chem. Phys.* **2006**, *124*, 1–12.
(18) Ault, B. S. *Acc. Chem. Res.* **1982**, *15*, 103–109.
(19) Gomez, H.; Meloni, G.; Madrid, J.; Neumark, D. M. *J. Chem. Phys.* **2003**, *119*, 872–879.
(20) Kawaguchi, K. *J. Chem. Phys.* **1988**, *88*, 4186–4189.
(21) Hamilton, I. P.; Li, G. P. *Chem. Phys. Lett.* **2003**, *381*, 623–627.
(22) Li, G. P.; Hamilton, I. P. *Chem. Phys. Lett.* **2002**, *368*, 236–241.
(23) Li, G. P.; Reinhart, B.; Hamilton, I. P. *J. Chem. Phys.* **2001**, *115*, 5883–5890.
(24) Akrour, A.; Chikh, Z.; Djazi, F.; Elbannay, M.; Berruyer, F.; Bouchoux, G. *Int. J. Mass Spectrom.* **2007**, *267*, 63–80.
(25) Szulejko, J. E.; Fisher, J. J.; McMahon, T. B.; Wronka, J. *J. Mass Spectrom. Ion Processes.* **1988**, *83*, 147–161.
(26) Mathur, D. *Chem. Phys. Lett.* **1981**, *81*, 115–118.
(27) Ruckhaberle, N.; Lehmann, L.; Matejcik, S.; Illenberger, E.; Bouteiller, Y.; Periquet, V.; Museur, L.; Desfrancois, C.; Schermann, J. *J. Phys. Chem. A* **1997**, *101*, 9942–9947.
(28) Yin, H.; Yang, B.; Han, K.; He, G.; Guo, J.; Liu, C.; Gu, Y. *Phys. Chem. Chem. Phys.* **2000**, *2*, 5093–5097.
(29) Grabowski, S. *Ann. Rep. Prog. Chem.* **2006**, *102*, 131–165.
(30) Frisch, M. J. et al. Gaussian, Inc.: Wallingford, CT, 2004.
(31) Dennington, R., II; Keith, T.; Millam, J.; Eppinnett, K.; Hovell, W. L.; Gilliland, R. Semichem, Inc: Shawnee Mission, KS, 2003.
(32) Blondel, C.; Delsart, C.; Goldfarb, F. *J. Phys. B* **2001**, *34*, L281−L288.
(33) Smith, J. R.; Kim, J. B.; Lineberger, W. C. *Phys. Rev. A* **1997**, *55*, 2036.
(34) Ramond, T. M.; Davico, G. E.; Schwartz, R. L.; Lineberger, W. C. *J. Chem. Phys.* **2000**, *112*, 1158–1169.

JP8071074